J. Jpn. Soc. Microgravity Appl. Vol. 27 No. 1 2010 (3–10)

Original Article

Automatic Microgravity Flight System and Flight Testing Using a Small Unmanned Aerial Vehicle

Shin-Ichiro HIGASHINO[1] and Shotaro KOZAI[2]

Abstract

This paper presents the attempt to apply UAV (Unmanned Aerial Vehicle) technology to microgravity experiments. The 6-degree of freedom simulation model of an electric-motor-driven test-bed UAV of which span and weight are 2.4 m and 2.5 kg respectively is established, and the feasibility of microgravity flight is examined using the simulation model and two types of acceleration feedback systems, i.e., acceleration component feedback in body axes and wind axes. The simulation results show that less than 0.15 G environment can be reached for more than several seconds, and the quality of the G-level and the duration differs depending on the type of the feedback. The flight testing system has been also developed including the onboard control system, data communication system, and the ground station together with the test-bed vehicle. Flight tests using the acceleration component feedback in body axes are performed, and one the results shows that minimum G-level reached approximately 0.15 G as implied by the simulation though the adjustment of the control gains was not enough. This G-level may not be satisfactory for practical use at the moment, but the feasibility of the microgravity flight using UAVs is confirmed by the flight data.

Nomenclature

A	Wing aspect ratio
A_x, A_y, A_z	Acceleration components in body axes
α, β	Angle of attack and side-slip angle
b	Span
$\bar{c}$	Mean aerodynamic chord length
C_L	Lift coefficient
C_{L_α}, C_{L_Q}, $C_{L_{\delta e}}$	Lift curve slope and stability derivatives (ex. $C_{L_\alpha}=\partial C_L/\partial\alpha$)
C_{D_0}	Zero lift drag coefficient
C_{l_β}, C_{l_P}, C_{l_R}, $C_{l_{\delta a}}$, $C_{l_{\delta r}}$	Stability derivatives regarding rolling moment (ex. $C_{l_\beta}=\partial C_l/\partial\beta$, where C_l is nondimensional rolling moment coefficient)
C_{m_0}	Constant nondimensional pitching moment coefficient
C_{m_α}, $C_{m_{\dot\alpha}}$, C_{m_Q}, $C_{m_{\delta e}}$	Stability derivatives regarding pitching moment (ex. $C_{m_\alpha}=\partial C_m/\partial\alpha$, where C_m is nondimensional pitching moment coefficient)
C_{n_β}, C_{n_P}, C_{n_R}, $C_{n_{\delta a}}$, $C_{n_{\delta r}}$	Stability derivatives regarding yawing moment (ex. $C_{n_\beta}=\partial C_n/\partial\beta$, where C_n is nondimensional yawing moment coefficient)
C_t	Thrust coefficient of a propeller
C_{y_β}, C_{y_P}, C_{y_R}, $C_{y_{\delta r}}$	Stability derivatives regarding side force (ex. $C_{y_\beta}=\partial C_y/\partial\beta$, where C_y is nondimensional side force coefficient)
D	Drag
δa, δe, δr	Control deflection angle of aileron, elevator, rudder
δt	Throttle position
e	Oswald factor
g	Gravity acceleration
I_x, I_y, I_z, I_{xz}	Moment of inertia and inertia product
L_i	Lift
L, M, N	Components of aerodynamic moments
m	Mass of the vehicle
P, Q, R	Angular velocity components
$\hat{P}$, $\hat{Q}$, $\hat{R}$	Nondimensional angular velocity components
q	Dynamic pressure
S	Wing area
T	Thrust
U, V, W	Velocity components
V_c	Trim speed
X_A, Y_Z, Z_A	Components of aerodynamic forces and thrust
Φ, Θ	Bank angle and pitch angle

1. Introduction

Rockets, manned airplanes, and drop towers are commonly used for the experiments[1–3] in microgravity

1 Department of Aeronautics and Astronautics, Kyushu University, 744 Moto-oka, Nishi-ku, Fukuoka 819–0395 Japan
2 Graduate Student, Kyushu University (Currently, Kawasaki Heavy Industries, LTD), 744 Moto-oka, Nishi-ku, Fukuoka 819–0395 Japan
(E-mail: tonton@aero.kyushu-u.ac.jp)

environment on earth. Although these methods have differences in reachable degree and quality of microgravity, obtainable time for microgravity, and cost, they all require relatively large scale experiment systems and high cost.

Meanwhile, many Unmanned Aerial Vehicles (UAVs) are developed and used today not only for military purposes[4] such as surveillance, reconnaissance, and target tracking, but also for scientific missions such as meteorological observation and environmental data collection[5–7]. The authors have developed a general-purpose flight control module for fixed-wing UAVs[8], and an autonomous UAV system for scientific missions in Antarctica[6,7]. Autonomous UAVs are controlled by microcomputers onboard not by a human pilot, so it is not necessary to consider the safety and physiological issues of a human pilot. They can maneuver as precisely as planned, and repeat the same maneuver without fatigue.

On the basis of this background, the authors have attempted to apply this technology to the realization of microgravity experiments at low cost. Eventually the UAV microgravity flight system must be required large payload capacity to carry out practical experiments, but we have initiated this attempt utilizing a small electric-motor-driven model airplane for simplicity and low cost. The following sections will describe the test-bed vehicle, simulation model and control system for microgravity flight, development of the flight testing system, and the results of the flight tests.

2. Design and Evaluation of the Flight Control System for Microgravity Flight Using a Simulator

2.1 Development of a Flight Simulator

A low-cost electric-motor-driven model airplane with 2.4 (m) of span and 2.5 (kg) of weight shown in **Fig. 1** was chosen as the test-bed vehicle in order to make the vehicle size as small as possible for easy handling while accommodating onboard avionics including a flight control module in flight tests which will be described later. The specifications of the vehicle are shown in **Table 1**.

A set of conventional nonlinear 6-DOF (Degree Of Freedom) equations of motion[9] about the C.G. of the vehicle with regard to the body axes derived from the dynamics of a rigid body is used for the simulation model as shown in eq. (1)–eq. (6). Aerodynamic forces and moments other than drag force are modeled as linear using so called stability derivatives as eq. (8)–eq. (12). Drag force is modeled as the sum of the linear part and nonlinear part due to the induced drag as shown in eq. (7).

Microgravity flight is considered to be appropriate to describe as nonlinear from the point of view of the vehicle motion, while aerodynamic forces and moments acting on the vehicle during the maneuver are considered to be linear because the maneuver does not require extreme change in forces and moments like stall. Parameters in eq. (1)–eq. (12) are estimated using DATCOM[10] and the measured parameters regarding the test-bed vehicle.

Fig. 1 Test-bed Vehicle.

Table 1 Specifications of the Test-bed Vehicle

Specifications	value
Span (m)	2.40
Gross Weight (kg)	2.50
Wind Area (m^2)	0.40
Mean Aerodynamic Chord Length (m)	0.17
Maximum Motor RPM	8000

$$m(\dot{U}+QW-RV)=X_A-mg\sin\Theta \quad (1)$$
$$m(\dot{V}+RU-PW)=Y_A+mg\sin\Phi\cos\Theta \quad (2)$$
$$m(\dot{W}+PV-QU)=Z_A+mg\cos\Phi\cos\Theta \quad (3)$$
$$I_x\dot{P}-I_{zx}(\dot{R}+PQ)-(I_y-I_Z)QR=L \quad (4)$$
$$I_y\dot{Q}-I_{zx}(R^2-P^2)-(I_z-I_x)RP=M \quad (5)$$
$$I_z\dot{R}-I_{zx}(\dot{P}-QR)-(I_x-I_y)PQ=N \quad (6)$$

Where

$$X_A=qS\{(C_{L_\alpha}\alpha+C_{L_{\hat{Q}}}\hat{Q}+C_{L_{\delta e}}\delta e)\sin\alpha-(C_{D_0}+C_L^2/\pi Ae)\cos\alpha+C_t\} \quad (7)$$
$$Y_A=qS(C_{y_\beta}\beta+C_{y_{\hat{P}}}\hat{P}+C_{y_{\hat{R}}}\hat{R}+C_{y_{\delta r}}\delta r) \quad (8)$$
$$Z_A=-qS\{(C_{L_\alpha}\alpha+C_{L_{\hat{Q}}}\hat{Q}+C_{L_{\delta e}}\delta e)\cos\alpha+(C_{D_0}+C_L^2/\pi Ae)\sin\alpha\} \quad (9)$$
$$L=qSb(C_{l_\beta}\beta+C_{l_{\hat{P}}}\hat{P}+C_{l_{\hat{R}}}\hat{R}+C_{l_{\delta a}}\delta a+C_{l_{\delta r}}\delta r) \quad (10)$$
$$M=qS\bar{c}(C_{m_0}+C_{m_\alpha}\alpha+C_{m_{\hat{\alpha}}}\hat{\alpha}+C_{m_{\hat{Q}}}\hat{Q}+C_{m_{\delta e}}\delta e) \quad (11)$$
$$M=qSb(C_{n_\beta}\beta+C_{n_{\hat{P}}}\hat{P}+C_{n_{\hat{R}}}\hat{R}+C_{n_{\delta a}}\delta a+C_{n_{\delta r}}\delta r) \quad (12)$$

2.2 Design and Evaluation of the Control System

2.2.1 Acceleration Component Feedback in Body Axes

In the microgravity flights using manned airplanes, microgravity is usually realized by the manual feedback of the reading of an accelerometer by a pilot[2], and it is natural to design flight control law using feedback of the accelerations. Here we attempt to realize

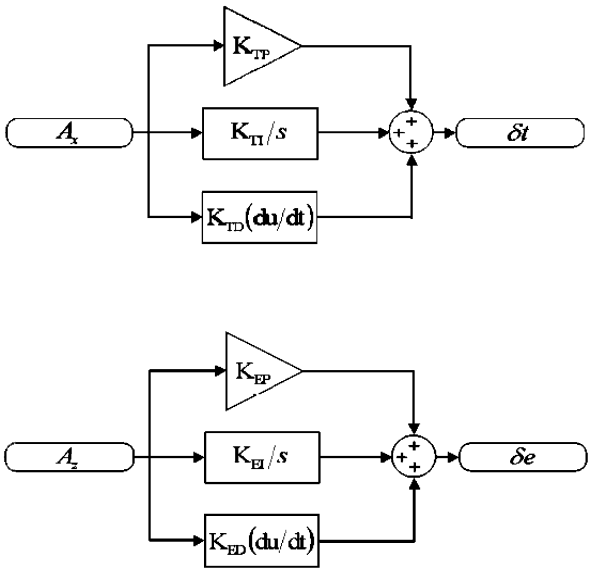

Fig. 2 Block diagram of the PID control using acceleration component feedback in body axes.

automatic microgravity flight of an UAV by manipulating throttle (δt) for the control of x-component of the acceleration vector in body axes (A_x, fore and aft direction), and an elevator (δe) for the control of z-component of the acceleration vector in body axes (A_z, vertical direction) using PID controllers as shown in **Fig. 2**. Body axes is defined as the vehicle-attached right-hand coordinate system with its origin at the center of gravity of the vehicle, and x-axis directs a certain fixed forward direction, y-axis directs right wing, and z-axis directs its belly. In Fig. 2, K_{TP}, K_{TI}, and K_{TD} are proportional, integral, and differential gains for throttle control respectively, and K_{EP}, K_{EI}, and K_{ED} are also proportional, integral, and differential gains for elevator control respectively. These control gains are determined considering stability of the feedback system, response time, and damping characteristics.

The quality and duration of microgravity is evaluated using the control system and the simulator described in section 2.1. Two types of maneuver, i.e. dive and parabolic flight both from trimmed level flight are evaluated here. We define G-level index as

$$G-level\ (G)=\frac{\sqrt{A_x^2+A_y^2+A_z^2}}{g} \tag{18}$$

in order to evaluate the magnitude of the acceleration.

The simulation results of dive maneuver from trimmed level flight for 8 seconds are shown in **Fig. 3–Fig. 5**. Fig. 3 shows the time history of the acceleration components and the G-level, **Fig. 4** shows the time history of elevator deflection and motor RPM, and Fig. 5 shows the time history of altitude and airspeed respectively. The simulation is initiated from trimmed level flight with 15 m/s of airspeed, and the acceleration command is given as $A_x=A_z=0$ three seconds after the beginning of the simulation. In Fig. 3, acceleration components are expressed in body axes,

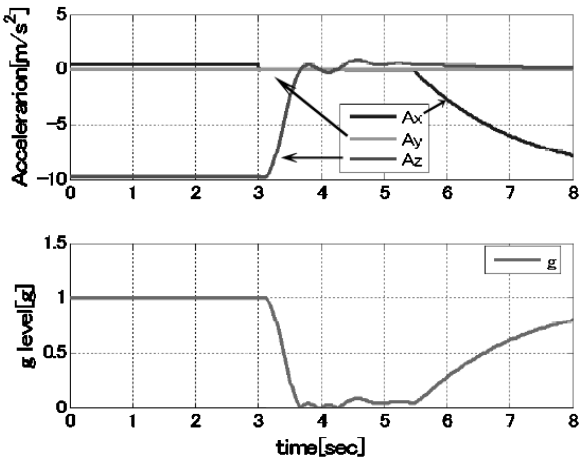

Fig. 3 Time history of acceleration components and G-level in the dive maneuver.

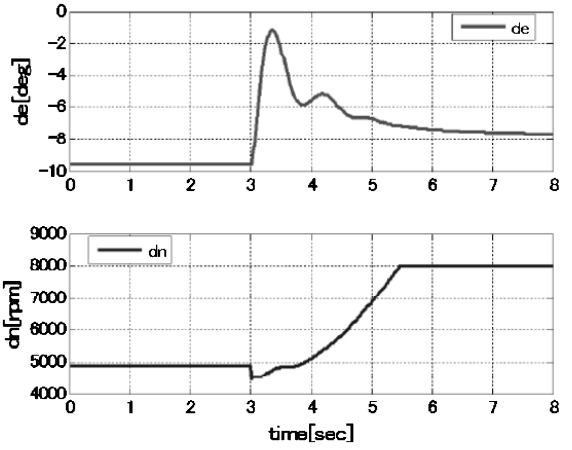

Fig. 4 Time history of elevator deflection (*de*) and motor RPM (*dn*) in dive maneuver.

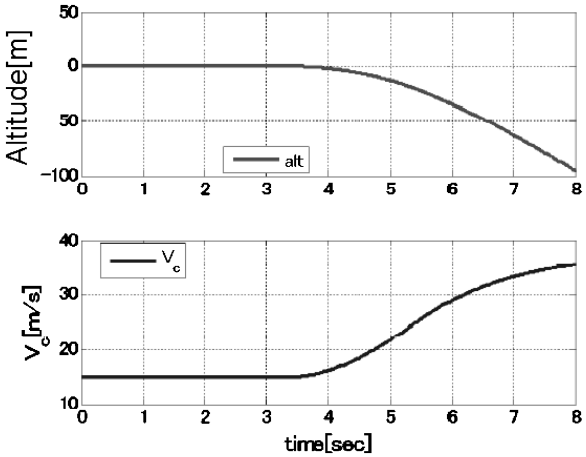

Fig. 5 Time history of altitude and airspeed (*Vc*) in dive maneuver.

Table 2 The magnitude of G-level and corresponding duration in dive maneuver

Magnitude of G-level (g)	Duration (sec)
G-level < 0.05	0.8
G-level < 0.1	2.0
G-level < 0.15	2.1

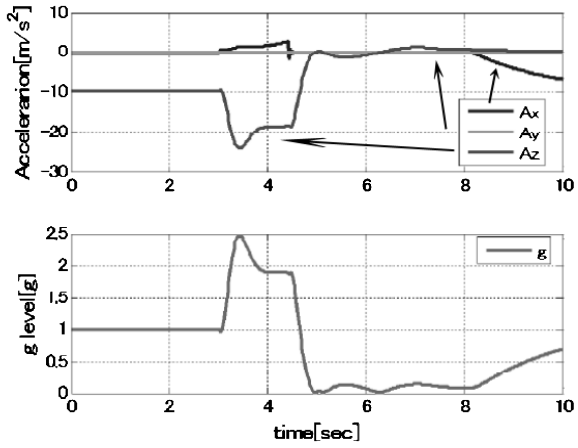

Fig. 6 Time history of acceleration components and G-level in the parabolic maneuver.

and A_z in steady level flight is expressed as negative value ($\fallingdotseq -9.8\ \mathrm{m/s^2}$). It can be seen from Fig. 3 that the acceleration environment less than 0.1 g lasts for about 2.0 seconds as summarized in **Table 2**. Fig. 3 and Fig. 4 show that x- and z-acceleration is controlled by throttle and elevator deflection, and x-acceleration cannot be kept close to zero about 2.5 seconds after the initiation of dive maneuver due to the RPM limit of the motor. From Fig. 5, it is seen that the altitude difference and airspeed difference between the start and end of the maneuver have no practical issues.

The simulation results using parabolic maneuver are shown similarly in **Fig. 6–Fig. 8**. Fig. 6 shows the time history of the acceleration components and the G-level, **Fig. 7** shows the time history of elevator deflection and motor RPM, and Fig. 8 shows the time history of altitude and airspeed respectively. The maneuver is initiated from trimmed level flight, and maximum motor RPM command (8000RPM) and acceleration command $A_z = -19.6\ (\mathrm{m/s^2})$ are given three seconds after the start of the simulation, then the acceleration command $A_x = A_z = 0$ are given at a certain time so that the minimum airspeed becomes 15 m/s. It is seen from Fig. 6 that the time in which the G-level is less than 0.15 g becomes longer (3.5 sec) than that in the dive maneuver as expected because the gravity acceleration acting in x-component of the body axes has deceleration effect, and the time to saturate RPM becomes longer. However, the time in which the G-level is less than

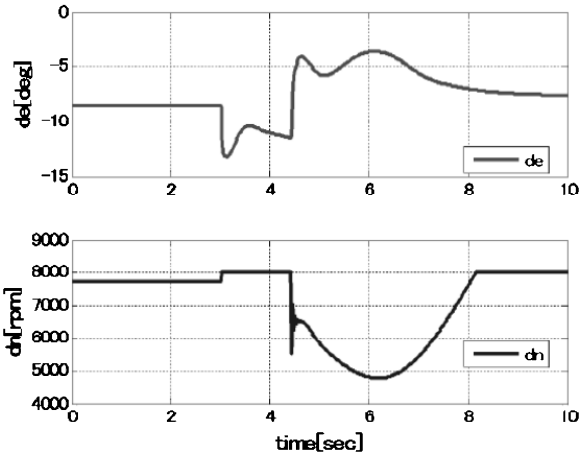

Fig. 7 Time history of elevator deflection (*de*) and motor RPM (*dn*) in parabolic maneuver.

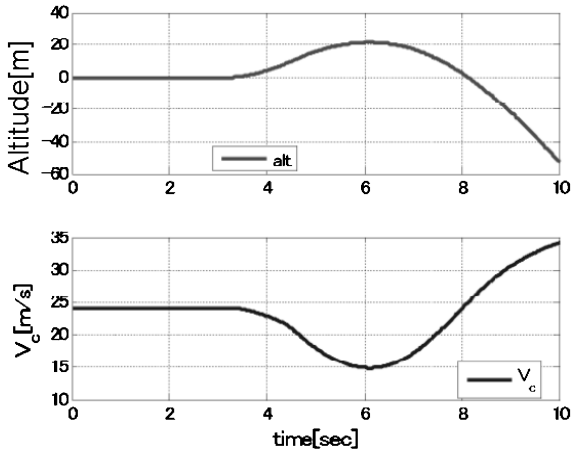

Fig. 8 Time history of altitude and airspeed (*Vc*) in parabolic maneuver.

Table 3 The magnitude of G-level and corresponding duration in parabolic maneuver

Magnitude of G-level (g)	Duration (sec)
G-level < 0.05	0.4
G-level < 0.1	0.9
G-level < 0.15	3.5

0.1 g is 0.9 sec as summarized in **Table 3**, and the time becomes shorter than that in previous dive maneuver. Fig. 7 and Fig. 8 shows that the maneuver is realizable with practical boundary of elevator deflection, altitude and airspeed difference at the both end of the maneuver. However, it is desirable to replace the motor by more powerful one in order to raise the RPM limit. It can be said that microgravity flight using a small UAV is feasible using both maneuvers, but the quality and duration differs depending on the type of the maneuver.

2.2.2 Acceleration Component Feedback in Wind Axes

In order to improve the time in which the G-level is kept small enough, we attempt to modify the control law. From longitudinal equations of motion eq. (1) and eq. (3), x- and z-acceleration components in body axes are expressed as

$$A_x = \frac{X_A}{m} = \dot{U} + QW - RV + g \sin \Theta \tag{19}$$

$$A_z = \frac{Z_A}{m} = \dot{W} + PV - QU - mg \cos \Phi \cos \Theta \tag{20}$$

Eq. (19) and eq. (20) shows that aerodynamic forces including thrust in body axes X_A and Z_A have to be as small as possible in order to make the accelerations A_x and A_x small. The aerodynamic forces X_A and Z_A in body axes are expressed using lift L_i, drag D in wind axes, and thrust T as

$$X_A = T + L_i \sin \alpha - D \cos \alpha \tag{21}$$

$$Z_A = -L_i \cos \alpha - D \sin \alpha \tag{22}$$

Wind axes is also defined as the vehicle-attached right-hand coordinate system with its origin at the center of gravity of the vehicle, but x-axis directs relative wind vector and consequently moves along the movement of the relative wind, y-axis directs right wing and is perpendicular to x-axis, and z-axis directs its belly.

Rearranging eq. (21) and eq. (22), The aerodynamic forces including thrust $X_{A_{wind}}$ and $Z_{A_{wind}}$ in wind axes are

$$X_{A_{wind}} = T \cos \alpha - D = m(A_x \cos \alpha + A_z \sin \alpha) \tag{23}$$

$$Z_{A_{wind}} = T \sin \alpha + L_i = m(A_x \sin \alpha - A_z \cos \alpha) \tag{24}$$

In an airplane, elevator deflection controls lift and drag which act on a vehicle perpendicular and parallel to z- and x-axis in wind axes. Motor RPM controls thrust, and thrust is considered to be almost aligned to x-axis in wind axes since angle of attack is very small in microgravity maneuver. Therefore we attempt to control the vehicle by feedback of x and z acceleration components in wind axes, i.e. $(A_x \cos \alpha + A_z \sin \alpha)$ feedback to motor RPM, and $(A_x \sin \alpha - A_z \cos \alpha)$ feedback to elevator deflection.

We introduce the load factor in x- and z-direction in wind axes as

$$lf_x = \frac{T \cos \alpha - D}{m} = A_x \cos \alpha + A_z \sin \alpha \tag{25}$$

$$lf_z = \frac{T \sin \alpha + L_i}{m} = A_x \sin \alpha - A_z \cos \alpha \tag{26}$$

The control system is modified as a PID control by the feedback of lf_x and lf_z as shown in **Fig. 9**. The control gains in Fig. 9 are also determined considering stability of the feedback system, response time, and damping characteristics.

The simulation results of dive maneuver from trimmed level flight using the modified control system are shown in **Fig. 10–Fig. 12**. The initial conditions

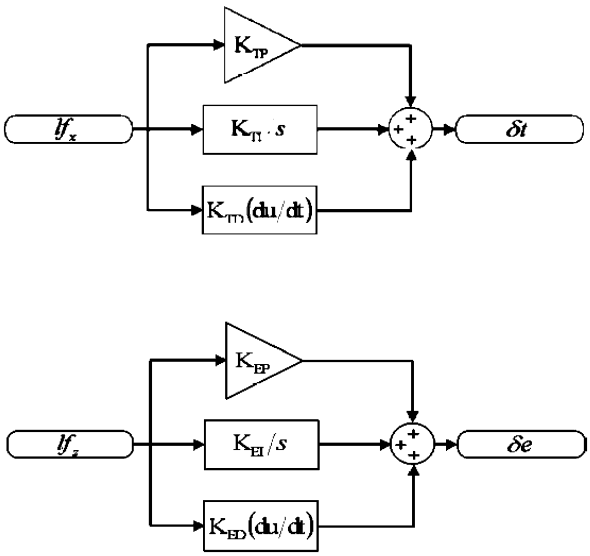

Fig. 9 Control System using load factor feedback.

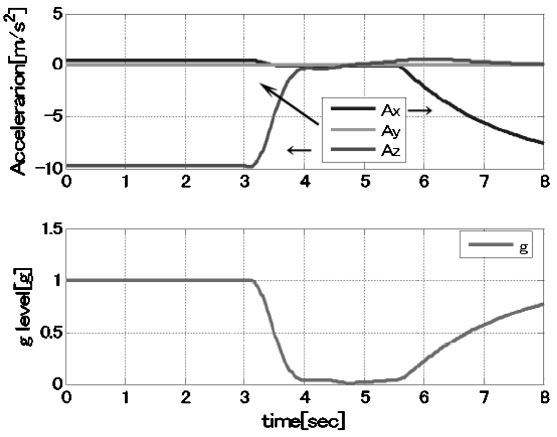

Fig. 10 Time history of acceleration components and G-level in the dive maneuver using modified control law.

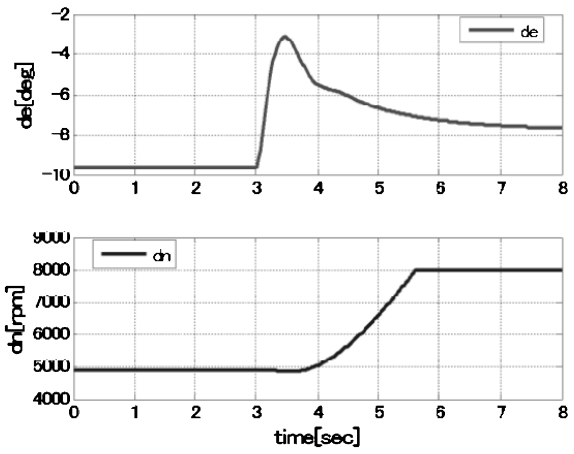

Fig. 11 Time history of elevator deflection (*de*) and motor RPM (*dn*) in dive maneuver using modified control law.

are the same as in the same dive maneuver using the acceleration feedback in body axes. Fig. 10 shows the time history of the acceleration components and the G-level, **Fig. 11** shows the time history of elevator deflection and motor RPM, and Fig. 12 shows the time history of altitude and airspeed respectively. Comparing Fig. 10 and Fig. 3, Overshoot and fluctuations in and G-level is being decreased using the modified control law. The time in which the G-level is less than 0.05 G becomes 1.7 seconds, and it is about twice as the corresponding time using the acceleration feedback in body axes. Fig. 11 and Fig. 12 shows that there are no particular issues regarding elevator deflection, altitude and airspeed difference at the both end of the maneuver. Fig. 11 indicates that it is desirable to replace the motor by a bigger one. The magnitude of G-level and corresponding duration in dive maneuver using modified control system is summarized in **Table 4**, and its performance is shown to be better than the acceleration feedback in body axes.

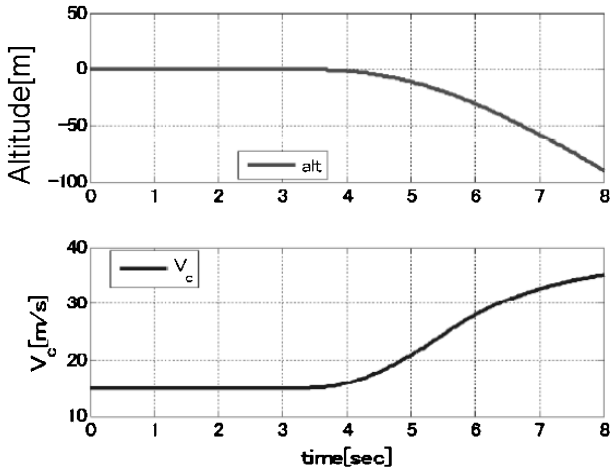

Fig. 12 Time history of altitude and airspeed (Vc) in dive maneuver using modified control law.

Table 4 The magnitude of G-level and corresponding duration in dive maneuver using modified control system

Magnitude of G-level (g)	Duration (sec)
G-level < 0.05	1.7
G-level < 0.1	1.9
G-level < 0.15	2.1

3. Evaluation by Flight Testing

3.1 Development of a Flight Testing System

Overview of the flight testing system developed based on our previously developed UAV system[6] is shown in **Fig. 13**. The flight control module[8] is composed of one sensor board and two CPU boards on

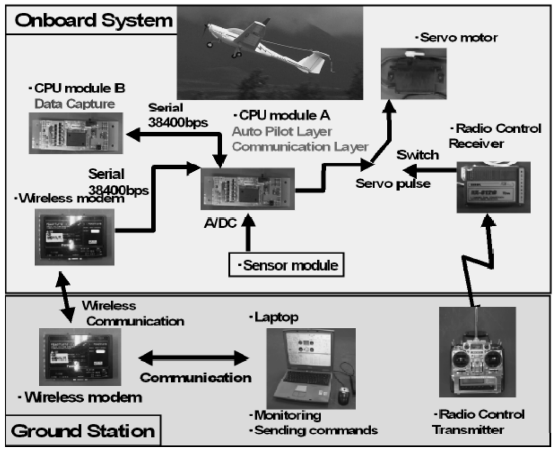

Fig. 13 Overview of the flight testing system.

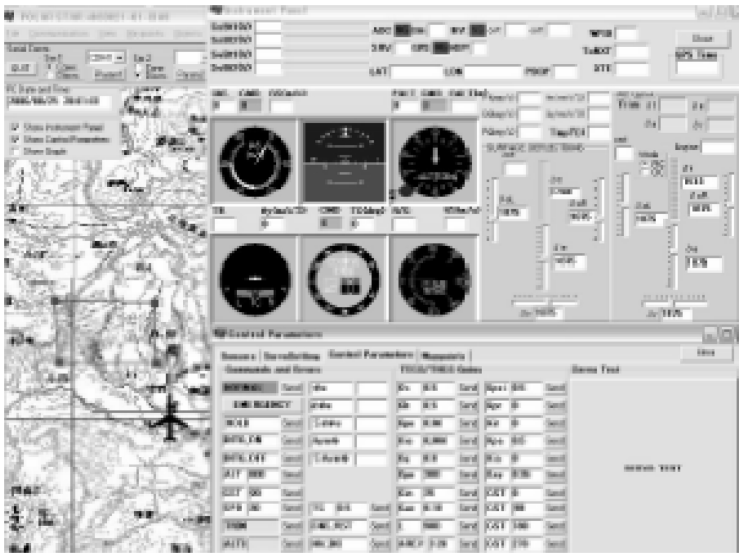

Fig. 14 Screenshot of the ground station software.

which a Renesus H82638 (20 MHz) CPU is mounted. The control law is implemented on the CPU board using C language, and it manipulates up to six servo actuators on the control surfaces and the motor. The sensor board has an absolute pressure sensor for pressure altitude measurement, a 3-axis angular rate sensor, and a 3-axis accelerometer on it. The accuracies of the accelerometers are 4.9×10^{-3} G in x- and y-direction, and 5.9×10^{-3} G in z-direction in body axes. The measured data are sampled at 50 Hz and used for the control. The data are also sent to a ground station lap-top at 25 Hz via a wireless modem and stored in the lap-top.

The operator not only monitors and saves transmitted flight data via wireless modem, but also initiate the maneuver and adjust control parameters even during flight using the ground station software. The software is developed taking advantage of the graphical user interface using C++ language as shown in **Fig. 14**.

3.2 Results of the Flight Tests

In flight tests, take-off of the UAV is manually done by a human pilot using radio control. After the vehicle is in level flight as shown in **Fig. 15(a)**, the control is switched to automatic control mode and the maneuver is initiated as shown in **Fig. 15(b)** and **(c)**. The control of the UAV is again switched to manual mode by the human pilot after the maneuver, and then the pilot pulls up as shown in **Fig. 15(d)** and lands the vehicle manually.

One of the results of the flight tests using the feedback of the acceleration components in body axes as shown in Fig. 2 and the dive maneuver is shown in **Fig. 16–Fig. 18**. The feedback of the acceleration components in wind axes is not implemented because it requires the development of an angle of attack sensor. Fig. 16 shows the time history of the acceleration components and the G-level. **Fig. 17** shows the time history of elevator deflection and motor RPM, and Fig. 18 shows the time history of altitude and airspeed respectively. The fluctuation in altitude seen in Fig. 18 is due to the resolution of the pressure altitude sensor (approximately 5.0 m). This resolution is relatively large, and it implies that the altitude during the first one second may have changed within the resolution, and it is considered that the G-level in initial part (approximately 0.7 G, not 1 G) may be caused due to the gradual altitude loss. In the flight tests, control gains are predetermined based on the simulation results and adjusted during flight seeing the test data. The adjustment was difficult because the operator has to adjust control gains in a very short time of the maneuver, and the adjustment was not enough. However, it is seen from Fig. 16 that the minimum G-level reaches approximately 0.15 G. Fig. 17 shows that the motor RPM reaches its maximum limit (8000RPM) in about one second, and x-acceleration deviates from 0 m/s^2

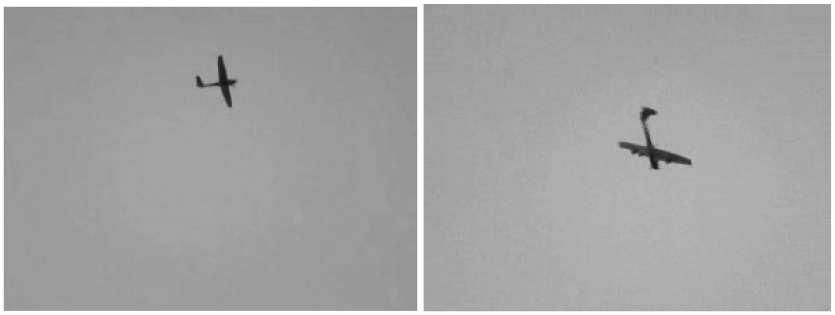

(a) Level flight (b) Initiation of dive maneuver

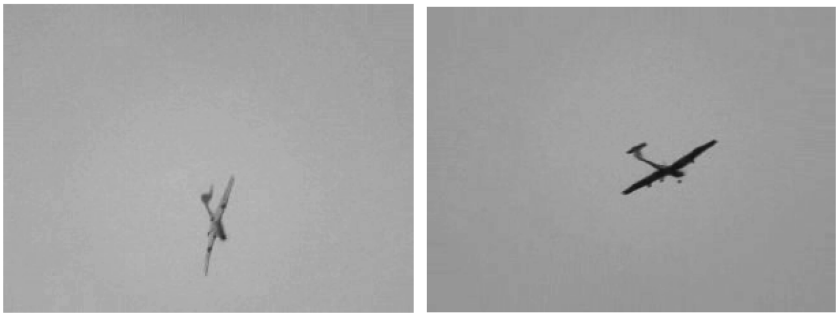

(c) Dive maneuver (d) Pull-up to level flight

Fig. 15 The UAV from level flight, dive maneuver to pull-up.

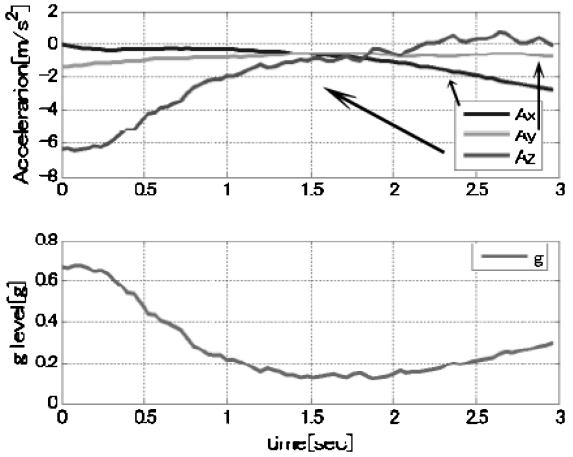

Fig. 16 Time history of acceleration components and G-level in the dive maneuver in the flight test.

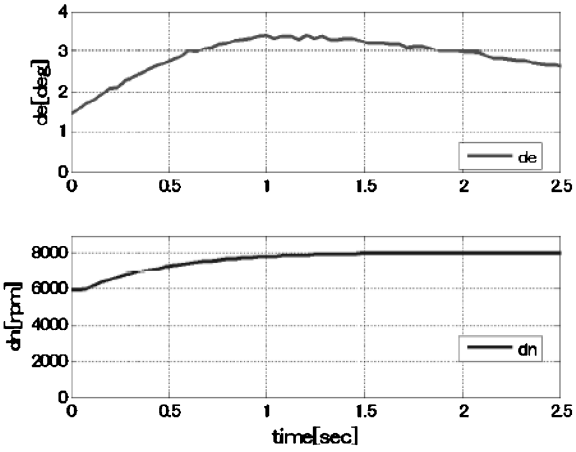

Fig. 17 Time history of elevator deflection (*de*) and motor RPM (*dn*) in dive maneuver in the flight test.

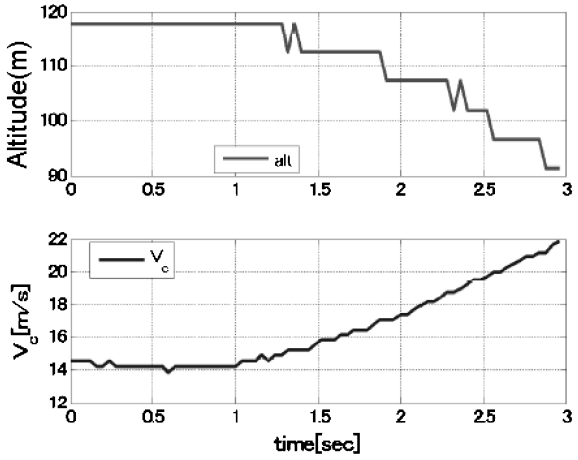

Fig. 18 Time history of altitude and airspeed (*Vc*) in dive maneuver in the flight test.

gradually due to the lack in thrust as shown in Fig. 16 similarly in the simulation. Although the minimum G-level realized here may not be small enough, it is shown that the microgravity flight using a small UAV is feasible. It is considered to be possible to improve minimum G-level by repeating flight tests and adjusting the control gains, and also modifying the control law as also implied by the simulation. Replacement of the motor to a bigger one is also required.

4. Conclusion

The authors have attempted to apply UAV technology to microgravity experiments. The 6-DOF (Degree Of Freedom) flight simulation model has been constructed for a small test-bed vehicle which utilizes an off-the-shelf products, and the feasibility of microgravity flight using an UAV is examined by the simulations. The simulation results show that microgravity environment less than approximately 0.1 G can be realized for a couple of seconds even using a small motor-driven UAV and a simple PID control system. The simulation results also show that the feedback of the acceleration components in wind axes is better than the feedback of the acceleration components in body axes in quality and duration of the microgravity.

Flight test system including automatic flight control system has been developed, and one of the results of the flight tests using the feedback of the acceleration components in body axes is shown. Although the adjustment of the control gains was not enough due to the short time for the adjustment, the smallest G-level realized in the test reached about 0.15 G. It may not be enough as the quality of microgravity level for practical use, however, it has been shown that the microgravity environment to that extent is easily realizable using even a small UAV.

References

1) R. J. Naumann: AIAA Paper, 3825, 1995.
2) A. M. (Alwin) Kraeger and M. M. (Rene) van Paassen: AIAA Paper, 4499, 2002.
3) J. M. Alford, G. R. Mason and D. A. Feikema: AIAA Paper, 1139, 2006.
4) http://www.nasm.si.edu/exhibitions/gal104/uav.cfm
5) B. L. Mulac, G. J. Holland, J. O. Pinto and J. A. Curry: AIAA Paper, 3476, 2002.
6) S. Higashino, M. Funaki and N. Hirasawa: AIAA Paper, 2761, 2007.
7) M. Funaki, N. Hirasawa, S. Imura, K. Moriwaki, Y. Nogi, K.Ishizawa, S. Higashino, H. Murase, S. Sakanaka and H. Sakai: Polar Science, **2** (2008) 129.
8) S. Higashino: Proc 5th Asian-Pacific Conference on Aerospace Technology and Science, Guilin, China, Nov. 2006 (CD-ROM).
9) B. Etkin and L. D. Reid: Dynamics of Flight—Stability and Control, **93**, John Wiley and Sons, Chapter 4 (1996) 93.
10) USAF Stability and Control DATCOM, Flight Control Division, Air Force Flight Dyanmics Laboratory, Wright-Patterson Air Force Base, Ohio, Jan. 1975.

(Received Oct. 2, 2009
Accepted for publication, Dec. 28, 2009)